Bull, J.M., De Mets, C., Krishna, K.S. and Sanderson, D.J. (2010). Reconciling plate kinematic and seismic estimates of lithospheric convergence in the central Indian Ocean. *Geology*, 38, (4), 307-310. (doi:10.1130/G30521.1).

See also Data Repository item 2010083

Reconciling plate kinematic and seismic estimates of lithospheric convergence in the central Indian Ocean

J.M. Bull[1], C. DeMets[2], K.S. Krishna[3], D.J. Sanderson[4], and S. Merkouriev[5]

[1]School of Ocean and Earth Science, National Oceanography Centre Southampton, University of Southampton, SO14 3ZH, UK

[2]Department of Geoscience, University of Wisconsin-Madison, Madison, WI 53706, USA

[3]National Institute of Oceanography, Council of Scientific and Industrial Research, Dona Paula, Goa – 403004, India

[4]School of Civil Engineering and the Environment, University of Southampton, Southampton, SO17 1BJ, UK

[5]SPbFIZMIRAN, Muchnoj per, 2, Box 188, St. Petersburg, Russia

ABSTRACT

The far-field signature of the India-Asia collision and history of uplift in Tibet is recorded by sediment input into the Indian Ocean and the strain accumulation history across the diffuse plate boundary between the Indian and Capricorn plates. We describe the history of India-Capricorn convergence from updated estimates of India-Somalia-Capricorn plate rotations and observations derived from seismic reflection data. New India-Capricorn plate rotations for the past 20 Myr are consistent with slow N-S convergence from 18 Ma about a stationary or nearly stationary pole near the eastern edge of the Chagos-Laccadive ridge, simpler than predicted by previous models based on many fewer data. The new rotations

suggest that convergence began between 18 Ma and 14 Ma, consistent with marine seismic evidence for an onset of deformation at 15.4 – 13.9 Ma. They further show that convergence rates doubled at 8 Ma, in agreement with a sharp increase in fault activity at 8 – 7.5 Ma seen on seismic reflection profiles. A discrepancy between the total strain estimated from kinematic and seismic reflection data can be reconciled if pervasive reverse faulting within the diffuse plate boundary is accompanied by block rotations of 1-3˚.

INTRODUCTION

The deformation zone within the central Indian Ocean is the best studied diffuse plate boundary zone in the Oceans (Fig. 1). The deformation is manifest on two spatial scales: reverse faulted blocks with 5 – 10 km spacing, and 100 km to 300-km-wavelength folding of the oceanic lithosphere. The deformation has been described by seismic reflection, heat flow, studies of intraplate seismicity as well as satellite gravity studies (e.g. Weissel et al., 1980; Bull and Scrutton, 1990a; Chamot-Rooke et al., 1993, Deplus et al., 1998; Delescluse et al., 2008; Delescluse and Chamot-Rooke, 2007). Motion across the diffuse plate boundary zone has been estimated independently from inversions of seafloor spreading rates and directions from the Carlsberg and Central Indian ridges and consists of counterclockwise rotation about a pole east of Chagos Bank (Royer and Gordon, 1997; Gordon et al., 1998; DeMets et al., 2005), such that convergence is predicted in the Central Indian and Wharton Basins, and extension west of Chagos Bank.

Seismic stratigraphic analysis of the Bengal Fan sediments has revealed that the main deformation phase began in the Miocene (8.0-7.5 Ma; Cochran, 1990) and included long wavelength folding, development of a regional unconformity, pervasive reverse faulting and continuation of long wavelength folding and faulting in the Pliocene (5.0-4.0 Ma) and

Pleistocene (0.8 Ma) (Krishna et al., 2001). Plate reconstructions independently confirm the onset of rapid deformation at 8-7 Ma (DeMets et al. 2005), and moreover suggest that significant, but slower deformation began as early as 20 Ma with large uncertainties. Seismic stratigraphic data (Krishna et al., 2009) suggest that slow deformation began at 15.4-13.9 Ma.

Although previous, independent analyses of seismic stratigraphic and plate kinematic data from the central Indian Ocean confirm important aspects of the style and timing of deformation across the wide plate boundary south of India, important discrepancies and uncertainties remain. For example, the most recent model for India-Capricorn plate motion (DeMets et al. 2005) predicts a systematic increase in the magnitude of N-S shortening across the India-Capricorn boundary zone east of the pole of rotation, whereas a recent analysis of seismic reflection data suggests a more complex pattern. Cumulative north south strain smaller than predicted from plate rotations has been found (Krishna et al., 2009), suggesting that unaccounted errors exist in one or both estimates, or that some deformation occurs either outside the diffuse boundary or via mechanisms not considered in these studies.

Here we derive new India-Capricorn finite rotations for the last 20 million years from recently published, high-resolution India-Somalia and Capricorn-Somalia rotations. We then compare these predictions with new shortening estimates from seismic reflection data that are based on rotations of reversely faulted blocks.

UPDATED PLATE KINEMATIC ESTIMATE

The new India-Capricorn-Somalia rotations (DR Tables 1-3, electronic supplement) are derived from new high-resolution estimates of India-Somalia motion since 20 Ma (Merkouriev and DeMets, 2006) and Capricorn-Somalia finite rotations from DeMets et al. (2005). The India-Somalia rotations are determined from an order-of-magnitude more magnetic anomaly crossings

than those of DeMets et al. (2005) and describe a simpler and better constrained post-20 Ma kinematic history than prior models. We corrected both sets of rotations for the effect of outward displacement, which shifts the mid-points of magnetic reversals several kilometers outward from spreading axes due to the finite width of the zone in which new seafloor acquires its magnetization (DeMets and Wilson 2008). Information about the methods used to estimate the new rotations is given in the accompanying electronic supplement.

Interval spreading rates determined from the updated Capricorn-Somalia and India-Somalia rotations (DR Fig. 1 in the supplement) illustrate the primary kinematic evidence for a change in India and Capricorn plate motions at 8-10 Ma, as discussed by Merkouriev and DeMets (2006). Spreading rates along both boundaries decreased by 25-30% from 20 Ma to ~10 Ma and then remained steady or increased slightly to the present. The newly estimated interval rates are less noisy than their predecessors (Merkouriev and DeMets, 2006) and clearly suggest two distinct stages of motion for both plate pairs since 20 Ma.

The new best-fitting India-Capricorn poles (Fig. 2 and DR Table 3 in the supplement) are all located within several hundred km of the eastern edge of the Chagos-Laccadive ridge and show no dependence on age. For example, the rotations that describe motion from the present to 8 Ma and from 8 Ma to 20 Ma (Fig. 1) differ insignificantly in location and predict that approximate north-south shortening dominated deformation nearly everywhere along the plate boundary during their respective time intervals. In contrast, the 20-8 Ma pole determined from rotations in DeMets et al. (2005) lies 1200 km NE of the 8-0 Ma estimate (Fig. 1) and predicts a component of extension across more than two-thirds of the India-Capricorn boundary before 8 Ma, in conflict with evidence for shortening at that time (Krishna et al. 2009). The new India-Capricorn rotation estimates therefore yield a simpler kinematic history that agrees better with the

independently determined shortening history across the diffuse plate boundary than was previously the case.

We interpret the new results as evidence that India-Capricorn motion since 20 Ma is well described by a stationary pole (at 3.7°S, 74.8°E in Fig. 1) located at the Fisher mean of the best-fitting rotations. That the stationary pole lies near the eastern edge of the Chagos-Laccadive ridge, which consists of unusually thick oceanic crust formed by the Reunion mantle plume (Henstock and Thompson, 2004), may indicate that the ridge plays a mechanical role in determining the pole location.

Using the stationary India-Capricorn pole described above, we apply procedures described by DeMets et al. (2005) to estimate an optimized time sequence of rotation angles (upper panel of Fig. 2). The new sequence of angles can be interpreted as evidence for either a two-stage or three-stage rotation history. Both include the previously reported, factor-of-two increase in India-Capricorn motion since 8 Ma (DeMets and Royer 2003; DeMets et al. 2005) and the three-stage rotation history subdivides motion before 8 Ma into periods of slow or possibly no motion before ~16±2 Ma and somewhat faster motion from ~16±2 Ma to 8 Ma. Inversions of the angles in Fig. 2 to estimate best-fitting slopes and ages for changes in motion for the two- and three-stage models indicate that a motion change at 7.8 Ma is highly significant, but that any earlier change cannot be distinguished reliably from the sparse and less certain angles for times before 13 Ma.

SEISMIC REFLECTION ANALYSIS

In the most recent synthesis of seismic reflection data (Krishna et al., 2009), measurements were made on the vertical separations of sedimentary horizons and unconformities on either side of 293 reverse faults. These data were then backstripped to determine fault activity histories. These

data indicate that near or prior to 20 Ma, isolated faults accommodated minor extensional movement before a period of tectonic quiescence. Compressional activity then began on individual fault blocks at 15.4 to 13.9 Ma and continued to 8.0 – 7.5 Ma. Strain rates increased abruptly at 8.0 – 7.5 Ma, which led to widespread reverse faulting and the formation of long wavelength undulations and the first regional unconformity, and has continued to present.

Previously, workers have calculated the cumulative shortening accommodated by reverse faulting across the diffuse plate boundary (Chamot-Rooke et al., 1993; Van Orman et al., 1995; Krishna et al., 2009) using a three-stage procedure. Vertical separations of sedimentary reflectors immediately above basement are first measured and depth-converted using the velocity law in Bull and Scrutton (1990b). These were assumed to approximate fault throws, and the horizontal (shortening) component was calculated using dips (36° – 45°) for the reverse faults in the top of the oceanic crust estimated from the seismic reflection data (e.g Bull and Scrutton, 1992 and Chamot-Rooke et al., 1993). This approach has yielded total strain estimates of 1.9% to 4.3% across the diffuse boundary. Long wavelength undulations in the central Indian Ocean accommodate < 1% of the total shortening across the diffuse plate boundary and are thus ignored in the following.

The procedure outlined above has three limitations that are likely to produce underestimates of the shortening - 1) the vertical separations are made in poorly imaged regions above and below the fault surface and incorporate drag; 2) the vertical separation is less than the throw for dipping horizons; and 3) the method ignores the likely contribution of fault block rotation to the estimated shortening. In the Central Indian Basin, seismic reflection data from faulted blocks (Fig. 3) clearly show that the top of layer 2 is rotated by 1° to 3° relative to horizontal (Fig. 3A), with

some fault blocks rotated by 6° to 8° (Fig. 3B). Previously published shortening estimates may thus underestimate the total shortening across the diffuse plate boundary.

We therefore recalculated shortening due to reverse faulting by applying a method widely used for rotational extensional faults – the 'domino' model of Wernicke and Burchfiel (1982). This provides an independent estimate of shortening without the problems inherent in determining heave from cutoffs at faults and incorporates the observed rotations. The method requires an estimate of the dip of each reverse fault and the rotation of each fault block (Fig. 3C), which can be approximated by the dip of the top of the oceanic crust. Reliable measurements of the latter are only feasible with multichannel seismic reflection data, which consistently images the top of basement (Bull and Scrutton, 1992; Chamot-Rooke et al., 1993). Multichannel data coverage is however much sparser than the single-channel data synthesized by Van Orman et al. (1995) and Krishna et al. (2009), thereby precluding an observationally-based correction for each fault that has been imaged in the diffuse plate boundary. We therefore re-estimated the total shortening for a range of plausible fault block rotations (ω=1°-3°), an average fault dip (δ) of 40°, and using profile lengths at each longitude defined by the distance between the most widely distributed faults (see Krishna et al., 2009). These give revised shortening of 2.1 % and 6.4%, which result in between 17 and 52 km of north-south convergence at 78.8˚E, increasing eastwards to between and 34 and 104 km of convergence at 87˚E (Fig. 4). The higher value exceeds previous maximum shortening estimates from seismic reflection data, most likely due to the problems described above in measuring vertical displacement across faults.

SYNTHESIS AND CONCLUSIONS

Here we summarise where our new plate kinematic analysis (Fig. 2) reconciles previous differences with seismic stratigraphic studies, and where differences remain. There is striking

agreement concerning the acceleration of convergence and associated contractional deformation at 8 Ma, with a well-defined factor-of-two increase in the rate of angular rotation contemporaneous with the development of a regional unconformity related to the formation of long wavelength (100 – 300 km) folds and an increase in reverse faulting activity seen on the seismic reflection profiles (Krishna et al. 2009). Both methods agree that convergence (and associated contractional deformation) began earlier and more slowly than 8 Ma. We show how a simple rotational model for reverse fault blocks can be used to reconcile the total amount of convergence across the diffuse plate boundary zone.

Additional work is needed to better resolve the history of India-Capricorn motion before 10 Ma. Whereas seismic stratigraphic-derived estimates indicate that convergence began at 15.4-13.9 Ma, the India-Capricorn rotation history allows for an onset of convergence as early as 18 Ma (Fig. 2). A conservative interpretation of these results is that slow convergence began between 18 Ma and 13.9 Ma. Better stratigraphic age control from a future Integrated Ocean Drilling Program (IODP) study site in the Bengal Fan is needed to reduce the uncertainty in our stratigraphic estimate, which relies on extrapolation of rates from a single drill site (ODP Leg 116). Analyses of additional magnetic anomalies are needed to improve the limited temporal resolution and uncertainties for rotations for times before 13 Ma, as well as test whether the negative rotation angle from 20-18 Ma, coinciding with a period of possible normal faulting observed by Krishna et al. (2009), is supported by additional reconstructions. Our new kinematic estimates do not reveal possible discrete phases of deformation at 5.0-4.0 Ma and 0.8 Ma inferred from seismic reflection data (Krishna et al. 2001), and are instead most simply interpreted as consistent with steady motion about a fixed pole since ~8 Ma (Fig. 2).

The cumulative shortening estimated by Krishna et al. (2009) from seismic reflection data (Fig. 4) is smaller than predicted by our updated and previous kinematic models for all four of the seismic profiles included in their analysis (Fig. 4), with differences of ~40 km for two profiles that greatly exceed the estimated uncertainties (±10 km). Given that all four profiles span almost all of the most intensely deforming areas of the plate boundary (Fig. 1), it seems unlikely that the discrepancy between the two independent shortening estimates can be attributed to structures not imaged by the seismic profiles. Similarly, the plate kinematic estimates are based on numerous unambiguous magnetic and bathymetric data and are both robust and have well characterized uncertainties.

We demonstrate here that previous shortening estimates from seismic reflection data were too low. Our new estimates of total shortening for assumed average fault block rotations of 2-3˚ and average fault dips of 40˚ (Fig. 4) bracket the shortening estimates predicted by our updated kinematic model, and thus fully reconcile the two independent estimates. Although not all the fault blocks show evidence for rotation and some fault blocks (e.g. Fig. 3B.) are rotated more than 3˚, we find it encouraging that such a simple geometric model can resolve the previously large discrepancy between the shortening estimates.

Reasons for the onset of convergence at 18 – 14 Ma are unclear, as are the causes of the sharp increase in deformation at 8 Ma – we know of no significant changes in spreading rates or directions at the Indian Ocean ridge system at these times. We follow other authors (e.g. Molnar and Stock, 2009; Gordon, 2009) in suggesting that the answers must lie within the history of Tibet, the uplift of which caused increased deviatoric stresses over a wide area including the Equatorial Indian Ocean. We note that a recent analysis of motion between the Indian and Eurasian plates (Molnar and Stock, 2009), although having less temporal resolution than our

study, is consistent with an event at 17 Ma causing a slowing of India-Eurasia convergence. That the India-Capricorn rotation pole since ~18 Ma has remained stationary and adjacent to the Chagos-Laccadive Ridge may indicate that the ridge has played a mechanical role in determining the pole location and hence deformation across the wide equatorial plate boundary.

ACKNOWLEDGEMENTS

We thank the Council of Scientific and Industrial Research and the Royal Society of London for their support. We thank Richard Gordon, Laurent Montesi, Patience Cowie and an anonymous reviewer for their careful and constructive comments, which significantly improved the manuscript. We are grateful to Steve Cande and Dave Rowley for changes they recommended to the supplementary materials.

REFERENCES CITED

Bull., J.M., and Scrutton, R.A., 1990a, Fault reactivation in the central Indian Ocean and the rheology of oceanic lithosphere: Nature, v. 344, p. 855-858.

Bull, J.M., and Scrutton, R.A., 1990b, Sediment velocities and deep structure from wide-angle reflection data around Leg 116 sites: in Cochran, J.R., Stow, D.A.V. et al., Proc. Ocean Drilling Program, Sci. Results Vol. 116, College Station, Texas, Ocean Drilling Program, 311-316.

Bull, J.M., and Scrutton, R.A., 1992, Seismic reflection images of intraplate deformation, central Indian Ocean, and their tectonic significance: Journal of the Geological Society of London, v. 149, p. 955-966.

Chamot-Rooke, N., Jestin, F., de Voogd, B., and Phedre Working Group, 1993, Intraplate shortening in the central Indian Ocean determined from a 2100-km-long north-south deep seismic reflection profile: Geology, v. 21, p. 1043-1046.

Cochran, J.R., 1990, Himalayan uplift, sea level, and the record of Bengal Fan sedimentation at the ODP Leg 116 sites, in Cochran, J.R., Stow, D.A.V., et al., Proceedings of the Ocean Drilling Program, Scientific results, Volume 116: College Station, Texas, Ocean Drilling Program, p. 397–414.

Delescluse, M., and Chamot-Rooke, N., 2007, Instantaneous deformation and kinematics of the India-Australia plate: Geophysical Journal International, v. 168, p. 818–842, doi: 10.1111/j.1365-246X.2006.03181.x.

Delescluse, M., Montési, L.G.J., and Chamot-Rooke, N., 2008, Fault reactivation and selective abandonment in the oceanic lithosphere: Geophysical Research Letters, v. 35, p. L16312, doi: 10.1029/2008GL035066.

DeMets, C., and J.-Y. Royer, 2003, A new high-resolution model for India-Capricorn motion since 20 Ma: Implications for the chronology and magnitude of distributed crustal deformation in the Central Indian Basin: Current Science, v. 85, p. 339-345.

DeMets, C., Gordon, R.G., and Royer, J-Y., 2005, Motion between the Indian, Capricorn and Somalian plates since 20 Ma: implications for the timing and magnitude of distributed lithospheric deformation in the equatorial Indian Ocean: Geophysical Journal International, v. 161, p. 445-468.

DeMets, C. and Wilson, D.S., 2008. Toward a minimum change model for recent plate motions: calibrating seafloor spreading rates for outward displacement: Geophysical Journal International, 174, 825-841, doi: 10.1111/j.1365-246X.2008.03836.x.

Deplus, C. et al., 1998, Direct evidence of active deformation in the eastern Indian oceanic plate: Geology, v. 26, p. 131-134.

Gordon, R.G., DeMets, C., and Royer, J-Y., 1998, Evidence for long-term diffuse deformation of the lithosphere of the equatorial Indian Ocean: Nature, v. 395, p. 370-374.

Gordon, R.G. , 2009, Lithospheric deformation in the equatorial Indian Ocean: Timing and Tibet: Geology, v. 37, p. 287-288.

Henstock, T.J., and Thompson, P.J., 2004. Self-consistent modeling of crustal thickness at Chagos-Laccadive Ridge from bathymetry and gravity data: Earth Planetary Science Letters, v. 224, p. 325-336. (doi:10.1016/j.epsl.2004.05.021)

Krishna, K.S., Bull, J.M., and Scrutton, R.A., 2001, Evidence for multiphase folding of the central Indian Ocean lithosphere: Geology, v. 29, p. 715-718.

Krishna, K.S., Bull, J.M., and Scrutton, R.A., 2009, Early (pre-8 Ma) fault activity and temporal strain accumulation in the central Indian Ocean: Geology, v. 37, p. 227-230.

Merkouriev, S. and DeMets, C. (2006). Constraints on Indian plate motion since 20 Ma from dense Russian magnetic data: Implications for Indian plate dynamics: Geochemistry, Geophysics, Geosystems, v. 7(2), Q02002 doi: 10.1029/2005GC001079. issn: 1525-2027.

Molnar, P., and Stock, J.M., 2009. Slowing of India's convergence with Eurasia since 20 Ma and its implications for Tibetan mantle dynamics: Tectonics, v. 28 TC3001, doi:10.1029/2008TC002271.

Royer, J-Y., and Gordon, R.G., 1997, The motion and boundary between the Capricorn and Australian plates: Science, v. 277, p. 1268-1274.

Van Orman, J., Cochran, J.R., Weissel, J.K., and Jestin, F., 1995, Distribution of shortening between the Indian and Australian plates in the central Indian Ocean: Earth Planetary Science Letters, v. 133, p. 35-46.

Weissel, J.K., Anderson, R.N., and Geller, C.A., 1980, Deformation of the Indo-Australian plate: Nature, v. 287, p. 284-291.

Wernicke, B., and Burchfiel, B.C., 1982, Modes of extensional tectonics: Journal of Structural Geology, v. 4, p. 105-115.

Figure 1. Location map of study area. Red circles show shallow earthquakes from 1963-2008, all magnitudes, from the U.S. National Earthquake Information Center data base. Red lines show

locations of seismic profiles described in the text. Solid blue star and circle show 8-0 Ma and 20-8 Ma Capricorn-India pole locations for this study, respectively. White star and circle labeled "D05" show Capricorn-India 8-0 Ma and 20-8 Ma poles from DeMets et al. (2005). Ellipses show two-dimensional, 1-sigma uncertainties. Inset shows extent of major plates and diffuse plate boundaries (stripes); CP – Capricorn; IN – Indian; SM – Somalia; AU – Australia.

Figure 2. Upper - India-Capricorn (In-Cp) finite rotation angles and standard errors for best-fitting poles from DR Table 4 and for 0-20 Ma stationary pole at 3.74˚S, 74.76˚E. Stationary pole angles are procedurally limited to magnetic reversals for which identical crossing points were used to reconstruct the Capricorn-Somalia (DeMets et al. 2005) and India-Somalia (Merkouriev and DeMets, 2006) plate positions. Gray lines indicate the best-fitting three-stage rotation history described in the text. Red and blue lines show the best-fitting, least-squares two-stage history for both sets of rotation angles. Ages for changes in motion were estimated as part of the inversion procedure and give a best age of 7.8±1 Ma. Lower - Predicted N-S shortening component across India-Capricorn plate boundary, 0-20 Ma. Shortening is predicted at 3.5˚S at the longitudes of four seismic profiles shown in Figure 1. Filled and open symbols are derived respectively from stationary-pole and best-fitting India-Capricorn rotations.

Figure 3. Seismic reflection images of tilted fault blocks bounded by reverse faults and the simple geometrical construction used to calculate shortening. (A) Fault block (representative of the deformational area) with a dip on the top of layer 2 of 2 - 3˚. TWT – two-way traveltime(B) Fault blocks showing the maximum amount of rotation with dip on the top of layer 2 of 4˚ to 8˚. Calculations of fault dip use velocity law of Bull and Scrutton (1990b). (C) Simple geometrical construction used to calculate shortening based solely on the dip of the reverse faults in the upper

296 part of the oceanic crust (δ), and the dip of the top of oceanic crust layer 2 (ω). See text for
297 discussion. L is fault block width; L_0 – original fault block width.

298 **Figure 4.** Cumulative shortening since 20 Ma predicted by the new fixed-pole model for India-
299 Capricorn (Ind-Cap) motion (black line) compared to simple geometrical models for different
300 angles of fault block rotation (Figure 3), and previous estimates of shortening derived from
301 seismic reflection data assuming average reverse fault dips of 40˚ in the oceanic crust. 1˚, 2˚ and
302 3˚ refer to the dip of the top of oceanic layer 2 (ω in Fig. 3). Error bars indicate the range for
303 observed fault dips 36˚-45˚ (Krishna et al., 2009; K et al., 2009 in figure).

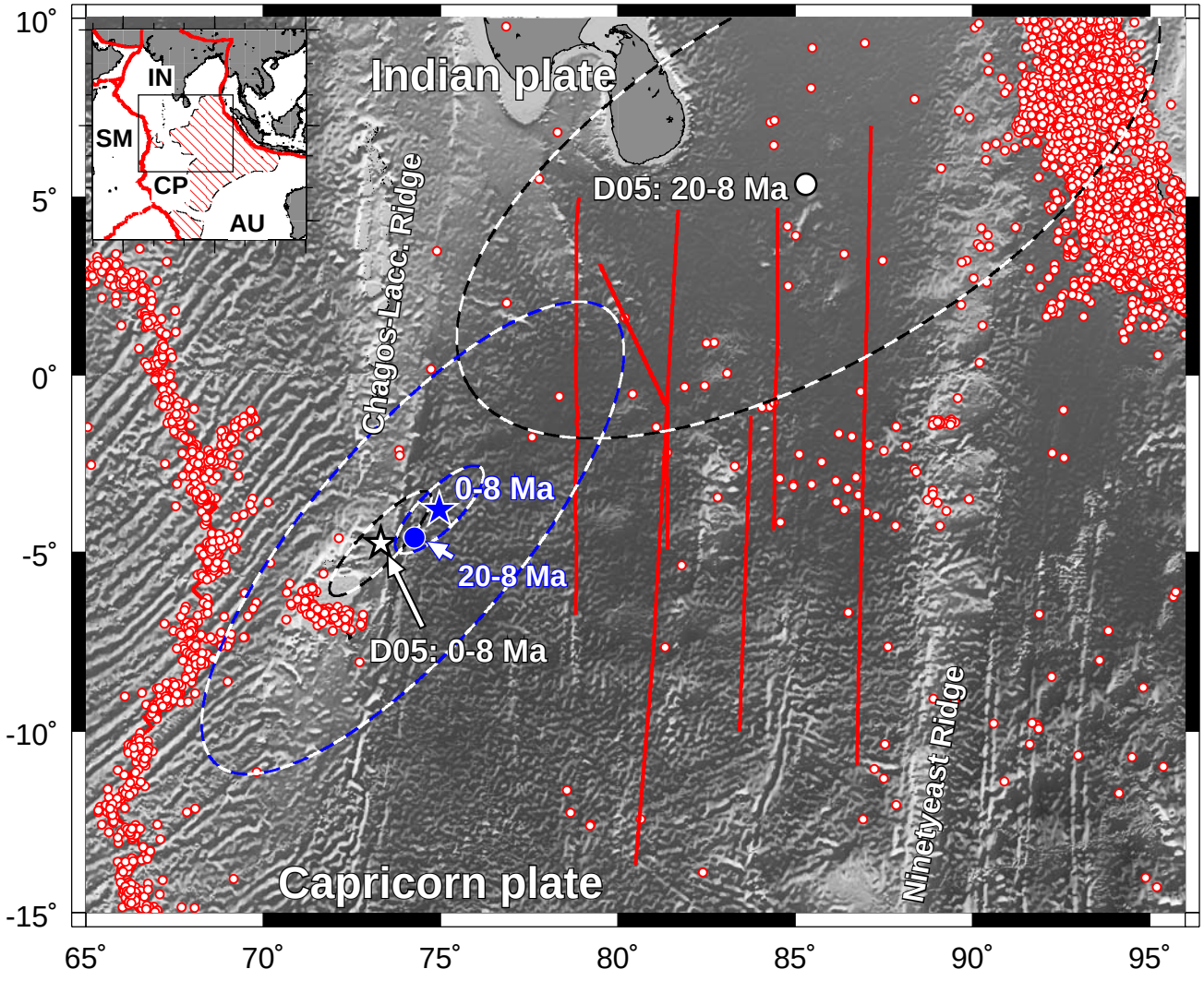

Figure 1. Location map of study area. Red circles show shallow earthquakes from 1963-2008, all magnitudes, from the U.S. National Earthquake Information Center data base. Red lines show locations of seismic profiles described in the text. Solid blue star and circle show 8-0 Ma and 20-8 Ma Capricorn-India pole locations for this study, respectively. White star and circle labeled "D05" show Capricorn-India 8-0 Ma and 20-8 Ma poles from DeMets et al. (2005). Ellipses show 2-D, 1-sigma uncertainties. Inset shows extent of major plates and diffuse plate boundaries (stripes).

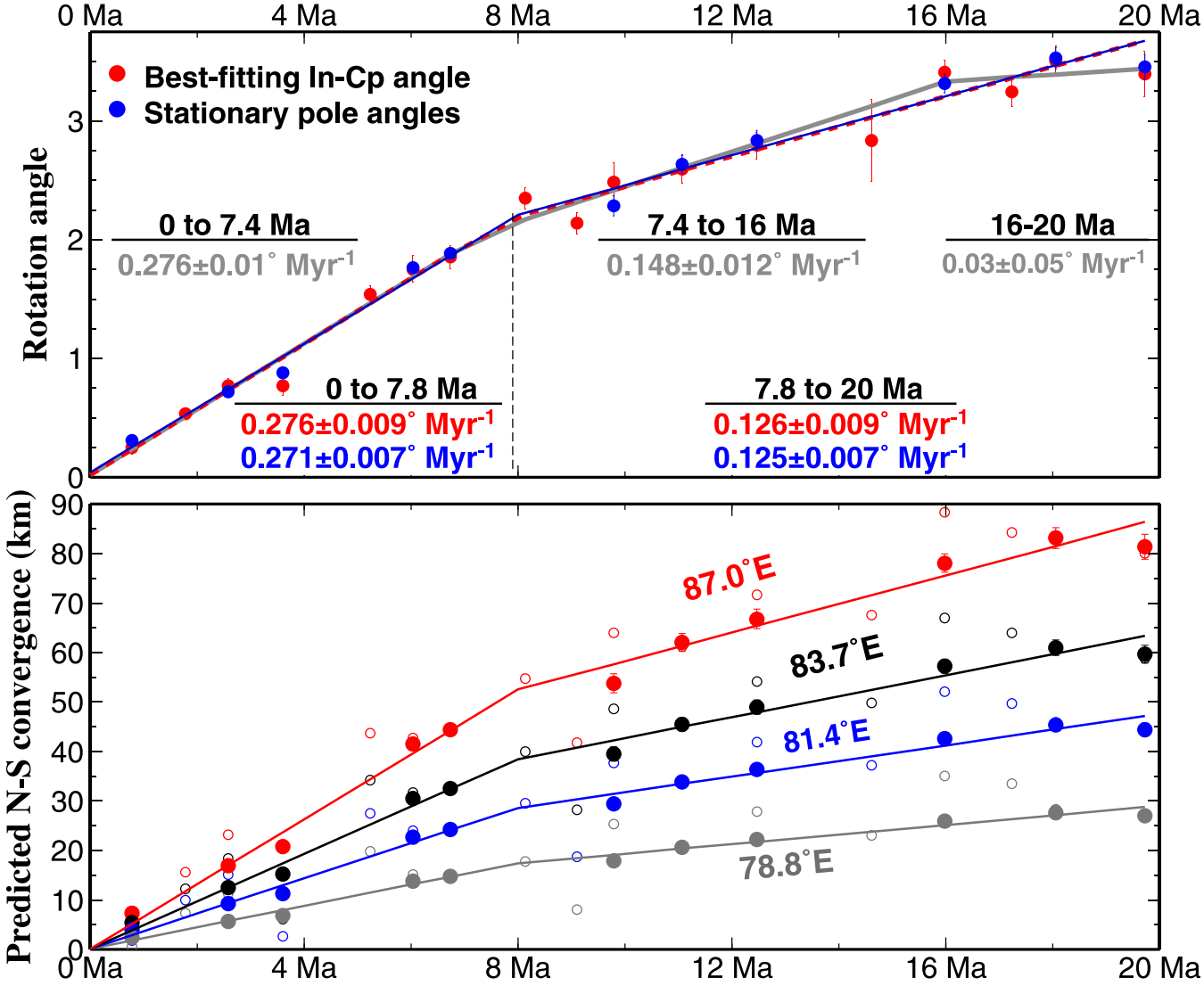

Figure 2. Upper - India-Capricorn finite rotation angles and standard errors for best-fitting poles from DR Table 4 and for 0-20 Ma stationary pole at 3.74 S, 74.76 E. Stationary pole angles are procedurally limited to magnetic reversals for which identical crossing points were used to reconstruct the Capricorn-Somalia (DeMets et al. 2005) and India-Somalia (Merkouriev and DeMets, 2006) plate positions. Gray lines indicate the best-fitting three-stage rotation history described in the text. Red and blue lines show the best-fitting, least-squares two-stage history for both sets of rotation angles. Ages for changes in motion were estimated as part of the inversion procedure and give a best age of 7.8±1Ma. Lower - Predicted N-S shortening component across India-Capricorn plate boundary, 0-20 Ma. Shortening is predicted at 3.5 S at the longitudes of four seismic profiles shown in Figure 1. Filled and open symbols are derived respectively from stationary-pole and best-fitting India-Capricorn rotations.

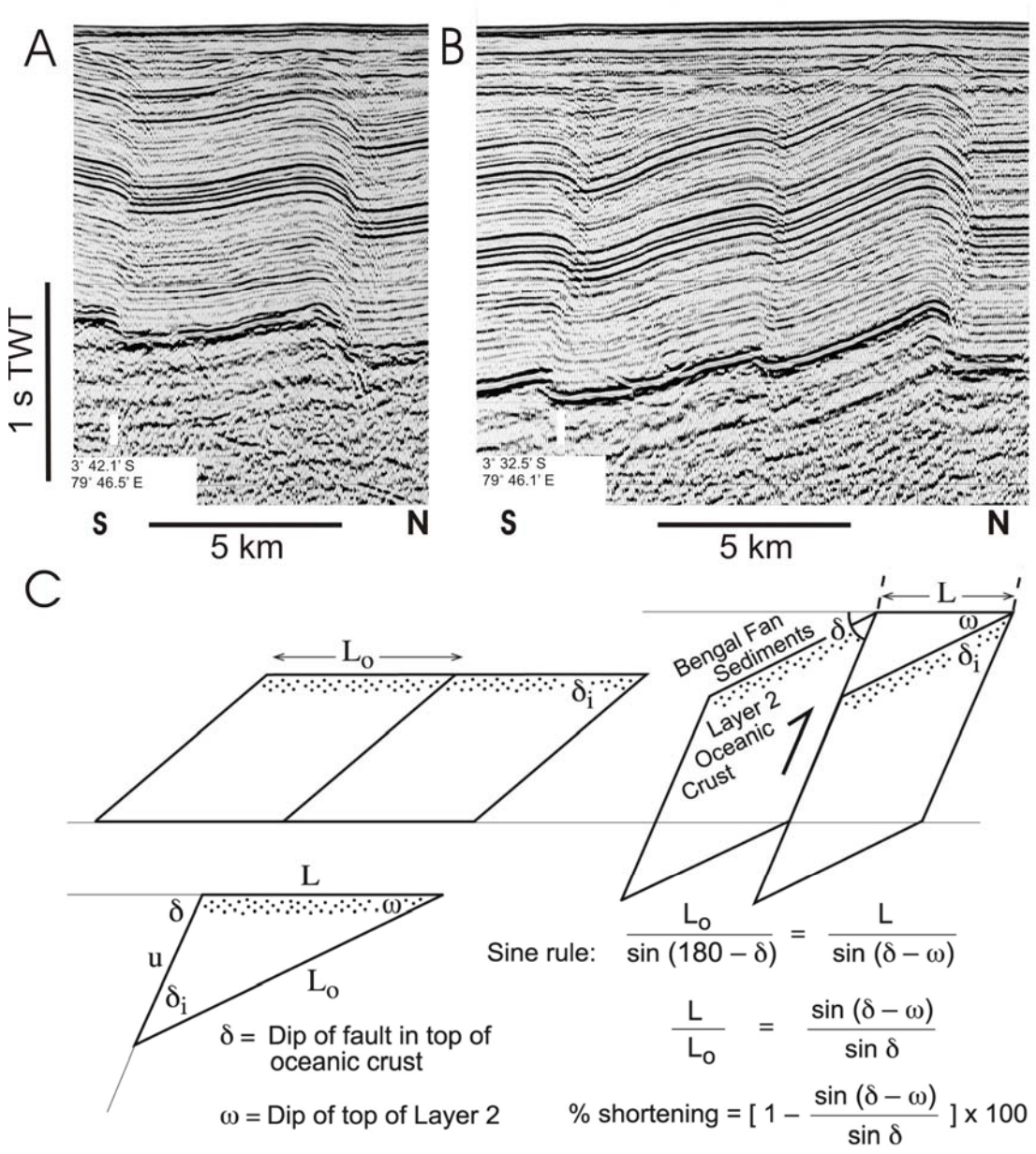

Figure 3. Seismic reflection images of tilted fault blocks bounded by reverse faults and the simple geometrical construction used to calculate shortening. (A) Fault block (representative of the deformational area) with a dip on the top of layer 2 of 2 - 3˚. TWT—two way traveltime. (B) Fault blocks showing the maximum amount of rotation with dip on the top of layer 2 of 4˚ to 8˚. Calculations of fault dip use velocity law of Bull and Scrutton (1990b). (C) Simple geometrical construction used to calculate shortening based solely on the dip of the reverse faults in the upper part of the oceanic crust (δ), and the dip of the top of oceanic crust layer 2 (ω). *L* is the fault block width, while L_0 is the original fault block width. (see text for discussion).

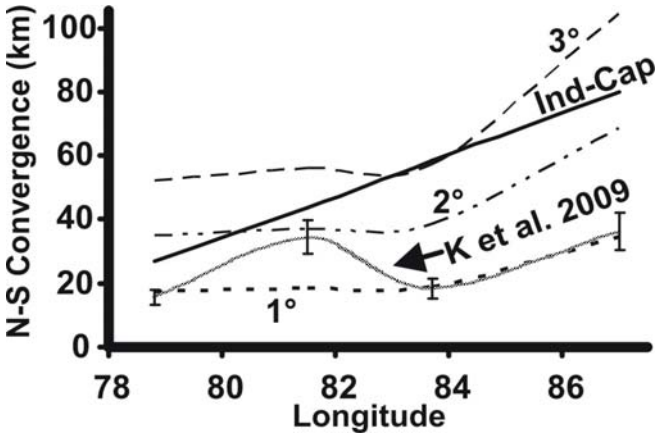

Figure 4. Cumulative shortening since 20 Ma predicted by the new fixed-pole model for India-Capricorn motion (black line) compared to simple geometrical models for different angles of fault block rotation (Figure 3), and previous estimates of shortening derived from seismic reflection data assuming average reverse fault dips of 40˚ in the oceanic crust. 1˚, 2˚ and 3˚ refer to the dip of the top of oceanic layer 2 (ω in Fig. 3). Error bars indicate the range for observed fault dips 36˚-45˚ (Krishna et al., 2009; K et al., 2009 in figure).